

Search for the rare charmless hadronic decay $B^+ \rightarrow a_0^+ \pi^0$

B. Aubert,¹ M. Bona,¹ D. Boutigny,¹ Y. Karyotakis,¹ J. P. Lees,¹ V. Poireau,¹ X. Prudent,¹ V. Tisserand,¹
A. Zghiche,¹ J. Garra Tico,² E. Grauges,² L. Lopez,³ A. Palano,³ M. Pappagallo,³ G. Eigen,⁴ B. Stugu,⁴
L. Sun,⁴ G. S. Abrams,⁵ M. Battaglia,⁵ D. N. Brown,⁵ J. Button-Shafer,⁵ R. N. Cahn,⁵ Y. Groyzman,⁵
R. G. Jacobsen,⁵ J. A. Kadyk,⁵ L. T. Kerth,⁵ Yu. G. Kolomensky,⁵ G. Kukartsev,⁵ D. Lopes Pegna,⁵ G. Lynch,⁵
L. M. Mir,⁵ T. J. Orimoto,⁵ I. L. Osipenkov,⁵ M. T. Ronan,^{5,*} K. Tackmann,⁵ T. Tanabe,⁵ W. A. Wenzel,⁵
P. del Amo Sanchez,⁶ C. M. Hawkes,⁶ A. T. Watson,⁶ T. Held,⁷ H. Koch,⁷ M. Pelizaeus,⁷ T. Schroeder,⁷
M. Steinke,⁷ D. Walker,⁸ D. J. Asgeirsson,⁹ T. Cuhadar-Donszelmann,⁹ B. G. Fulsom,⁹ C. Hearty,⁹ T. S. Mattison,⁹
J. A. McKenna,⁹ A. Khan,¹⁰ M. Saleem,¹⁰ L. Teodorescu,¹⁰ V. E. Blinov,¹¹ A. D. Bukin,¹¹ V. P. Druzhinin,¹¹
V. B. Golubev,¹¹ A. P. Onuchin,¹¹ S. I. Serednyakov,¹¹ Yu. I. Skovpen,¹¹ E. P. Solodov,¹¹ K. Yu. Todyshev,¹¹
M. Bondioli,¹² S. Curry,¹² I. Eschrich,¹² D. Kirkby,¹² A. J. Lankford,¹² P. Lund,¹² M. Mandelkern,¹²
E. C. Martin,¹² D. P. Stoker,¹² S. Abachi,¹³ C. Buchanan,¹³ S. D. Foulkes,¹⁴ J. W. Gary,¹⁴ F. Liu,¹⁴ O. Long,¹⁴
B. C. Shen,¹⁴ L. Zhang,¹⁴ H. P. Paar,¹⁵ S. Rahatlou,¹⁵ V. Sharma,¹⁵ J. W. Berryhill,¹⁶ C. Campagnari,¹⁶
A. Cunha,¹⁶ B. Dahmes,¹⁶ T. M. Hong,¹⁶ D. Kovalskyi,¹⁶ J. D. Richman,¹⁶ T. W. Beck,¹⁷ A. M. Eisner,¹⁷
C. J. Flacco,¹⁷ C. A. Heusch,¹⁷ J. Kroseberg,¹⁷ W. S. Lockman,¹⁷ T. Schalk,¹⁷ B. A. Schumm,¹⁷ A. Seiden,¹⁷
M. G. Wilson,¹⁷ L. O. Winstrom,¹⁷ E. Chen,¹⁸ C. H. Cheng,¹⁸ F. Fang,¹⁸ D. G. Hitlin,¹⁸ I. Narsky,¹⁸ T. Piatenko,¹⁸
F. C. Porter,¹⁸ R. Andreassen,¹⁹ G. Mancinelli,¹⁹ B. T. Meadows,¹⁹ K. Mishra,¹⁹ M. D. Sokoloff,¹⁹ F. Blanc,²⁰
P. C. Bloom,²⁰ S. Chen,²⁰ W. T. Ford,²⁰ J. F. Hirschauer,²⁰ A. Kreisel,²⁰ M. Nagel,²⁰ U. Nauenberg,²⁰ A. Olivas,²⁰
J. G. Smith,²⁰ K. A. Ulmer,²⁰ S. R. Wagner,²⁰ J. Zhang,²⁰ A. M. Gabareen,²¹ A. Soffer,^{21,†} W. H. Toki,²¹
R. J. Wilson,²¹ F. Winklmeier,²¹ D. D. Altenburg,²² E. Feltresi,²² A. Hauke,²² H. Jasper,²² J. Merkel,²²
A. Petzold,²² B. Spaan,²² K. Wacker,²² V. Klose,²³ M. J. Kobel,²³ H. M. Lacker,²³ W. F. Mader,²³ R. Nogowski,²³
J. Schubert,²³ K. R. Schubert,²³ R. Schwierz,²³ J. E. Sundermann,²³ A. Volk,²³ D. Bernard,²⁴ G. R. Bonneaud,²⁴
E. Latour,²⁴ V. Lombardo,²⁴ Ch. Thiebaux,²⁴ M. Verderi,²⁴ P. J. Clark,²⁵ W. Gradl,²⁵ F. Muheim,²⁵ S. Playfer,²⁵
A. I. Robertson,²⁵ J. E. Watson,²⁵ Y. Xie,²⁵ M. Andreotti,²⁶ D. Bettoni,²⁶ C. Bozzi,²⁶ R. Calabrese,²⁶ A. Cecchi,²⁶
G. Cibinetto,²⁶ P. Franchini,²⁶ E. Luppi,²⁶ M. Negrini,²⁶ A. Petrella,²⁶ L. Piemontese,²⁶ E. Prencipe,²⁶
V. Santoro,²⁶ F. Anulli,²⁷ R. Baldini-Ferrolì,²⁷ A. Calcaterra,²⁷ R. de Sangro,²⁷ G. Finocchiaro,²⁷ S. Pacetti,²⁷
P. Patteri,²⁷ I. M. Peruzzi,^{27,‡} M. Piccolo,²⁷ M. Rama,²⁷ A. Zallo,²⁷ A. Buzzo,²⁸ R. Contri,²⁸ M. Lo Vetere,²⁸
M. M. Macri,²⁸ M. R. Monge,²⁸ S. Passaggio,²⁸ C. Patrignani,²⁸ E. Robutti,²⁸ A. Santroni,²⁸ S. Tosi,²⁸
K. S. Chaisanguanthum,²⁹ M. Morii,²⁹ J. Wu,²⁹ R. S. Dubitzky,³⁰ J. Marks,³⁰ S. Schenk,³⁰ U. Uwer,³⁰ D. J. Bard,³¹
P. D. Dauncey,³¹ R. L. Flack,³¹ J. A. Nash,³¹ W. Panduro Vazquez,³¹ M. Tibbetts,³¹ P. K. Behera,³² X. Chai,³²
M. J. Charles,³² U. Mallik,³² V. Ziegler,³² J. Cochran,³³ H. B. Crawley,³³ L. Dong,³³ V. Eyges,³³ W. T. Meyer,³³
S. Prell,³³ E. I. Rosenberg,³³ A. E. Rubin,³³ Y. Y. Gao,³⁴ A. V. Gritsan,³⁴ Z. J. Guo,³⁴ C. K. Lae,³⁴ A. G. Denig,³⁵
M. Fritsch,³⁵ G. Schott,³⁵ N. Arnaud,³⁶ J. Béquilleux,³⁶ A. D'Orazio,³⁶ M. Davier,³⁶ G. Grosdidier,³⁶ A. Höcker,³⁶
V. Lepeltier,³⁶ F. Le Diberder,³⁶ A. M. Lutz,³⁶ S. Pruvot,³⁶ S. Rodier,³⁶ P. Roudeau,³⁶ M. H. Schune,³⁶
J. Serrano,³⁶ V. Sordini,³⁶ A. Stocchi,³⁶ W. F. Wang,³⁶ G. Wormser,³⁶ D. J. Lange,³⁷ D. M. Wright,³⁷
I. Bingham,³⁸ C. A. Chavez,³⁸ I. J. Forster,³⁸ J. R. Fry,³⁸ E. Gabathuler,³⁸ R. Gamet,³⁸ D. E. Hutchcroft,³⁸
D. J. Payne,³⁸ K. C. Schofield,³⁸ C. Touramanis,³⁸ A. J. Bevan,³⁹ K. A. George,³⁹ F. Di Lodovico,³⁹ W. Menges,³⁹
R. Sacco,³⁹ G. Cowan,⁴⁰ H. U. Flaecher,⁴⁰ D. A. Hopkins,⁴⁰ S. Paramesvaran,⁴⁰ F. Salvatore,⁴⁰ A. C. Wren,⁴⁰
D. N. Brown,⁴¹ C. L. Davis,⁴¹ J. Allison,⁴² N. R. Barlow,⁴² R. J. Barlow,⁴² Y. M. Chia,⁴² C. L. Edgar,⁴²
G. D. Lafferty,⁴² T. J. West,⁴² J. I. Yi,⁴² J. Anderson,⁴³ C. Chen,⁴³ A. Jawahery,⁴³ D. A. Roberts,⁴³ G. Simi,⁴³
J. M. Tuggle,⁴³ G. Blaylock,⁴⁴ C. Dallapiccola,⁴⁴ S. S. Hertzbach,⁴⁴ X. Li,⁴⁴ T. B. Moore,⁴⁴ E. Salvati,⁴⁴
S. Saremi,⁴⁴ R. Cowan,⁴⁵ D. Dujmic,⁴⁵ P. H. Fisher,⁴⁵ K. Koeneke,⁴⁵ G. Sciolla,⁴⁵ S. J. Sekula,⁴⁵ M. Spitznagel,⁴⁵
F. Taylor,⁴⁵ R. K. Yamamoto,⁴⁵ M. Zhao,⁴⁵ Y. Zheng,⁴⁵ S. E. Mclachlin,^{46,*} P. M. Patel,⁴⁶ S. H. Robertson,⁴⁶
A. Lazzaro,⁴⁷ F. Palombo,⁴⁷ J. M. Bauer,⁴⁸ L. Cremaldi,⁴⁸ V. Eschenburg,⁴⁸ R. Godang,⁴⁸ R. Kroeger,⁴⁸
D. A. Sanders,⁴⁸ D. J. Summers,⁴⁸ H. W. Zhao,⁴⁸ S. Brunet,⁴⁹ D. Côté,⁴⁹ M. Simard,⁴⁹ P. Taras,⁴⁹ F. B. Viaud,⁴⁹
H. Nicholson,⁵⁰ G. De Nardo,⁵¹ F. Fabozzi,^{51,§} L. Lista,⁵¹ D. Monorchio,⁵¹ C. Sciacca,⁵¹ M. A. Baak,⁵² G. Raven,⁵²
H. L. Snoek,⁵² C. P. Jessop,⁵³ K. J. Knoepfel,⁵³ J. M. LoSecco,⁵³ G. Benelli,⁵⁴ L. A. Corwin,⁵⁴ K. Honscheid,⁵⁴

H. Kagan,⁵⁴ R. Kass,⁵⁴ J. P. Morris,⁵⁴ A. M. Rahimi,⁵⁴ J. J. Regensburger,⁵⁴ Q. K. Wong,⁵⁴ N. L. Blount,⁵⁵ J. Brau,⁵⁵ R. Frey,⁵⁵ O. Igonkina,⁵⁵ J. A. Kolb,⁵⁵ M. Lu,⁵⁵ R. Rahmat,⁵⁵ N. B. Sinev,⁵⁵ D. Strom,⁵⁵ J. Strube,⁵⁵ E. Torrence,⁵⁵ N. Gagliardi,⁵⁶ A. Gaz,⁵⁶ M. Margoni,⁵⁶ M. Morandin,⁵⁶ A. Pompili,⁵⁶ M. Posocco,⁵⁶ M. Rotondo,⁵⁶ F. Simonetto,⁵⁶ R. Stroili,⁵⁶ C. Voci,⁵⁶ E. Ben-Haim,⁵⁷ H. Briand,⁵⁷ G. Calderini,⁵⁷ J. Chauveau,⁵⁷ P. David,⁵⁷ L. Del Buono,⁵⁷ Ch. de la Vaissière,⁵⁷ O. Hamon,⁵⁷ Ph. Leruste,⁵⁷ J. Malclès,⁵⁷ J. Ocariz,⁵⁷ A. Perez,⁵⁷ J. Prendki,⁵⁷ L. Gladney,⁵⁸ M. Biasini,⁵⁹ R. Covarelli,⁵⁹ E. Manoni,⁵⁹ C. Angelini,⁶⁰ G. Batignani,⁶⁰ S. Bettarini,⁶⁰ M. Carpinelli,⁶⁰ R. Cenci,⁶⁰ A. Cervelli,⁶⁰ F. Forti,⁶⁰ M. A. Giorgi,⁶⁰ A. Lusiani,⁶⁰ G. Marchiori,⁶⁰ M. A. Mazur,⁶⁰ M. Morganti,⁶⁰ N. Neri,⁶⁰ E. Paoloni,⁶⁰ G. Rizzo,⁶⁰ J. J. Walsh,⁶⁰ M. Haire,⁶¹ J. Biesiada,⁶² P. Elmer,⁶² Y. P. Lau,⁶² C. Lu,⁶² J. Olsen,⁶² A. J. S. Smith,⁶² A. V. Telnov,⁶² E. Baracchini,⁶³ F. Bellini,⁶³ G. Cavoto,⁶³ D. del Re,⁶³ E. Di Marco,⁶³ R. Faccini,⁶³ F. Ferrarotto,⁶³ F. Ferroni,⁶³ M. Gaspero,⁶³ P. D. Jackson,⁶³ L. Li Gioi,⁶³ M. A. Mazzoni,⁶³ S. Morganti,⁶³ G. Piredda,⁶³ F. Polci,⁶³ F. Renga,⁶³ C. Voena,⁶³ M. Ebert,⁶⁴ T. Hartmann,⁶⁴ H. Schröder,⁶⁴ R. Waldi,⁶⁴ T. Adye,⁶⁵ G. Castelli,⁶⁵ B. Franek,⁶⁵ E. O. Olaiya,⁶⁵ S. Ricciardi,⁶⁵ W. Roethel,⁶⁵ F. F. Wilson,⁶⁵ S. Emery,⁶⁶ M. Escalier,⁶⁶ A. Gaidot,⁶⁶ S. F. Ganzhur,⁶⁶ G. Hamel de Monchenault,⁶⁶ W. Kozanecki,⁶⁶ G. Vasseur,⁶⁶ Ch. Yèche,⁶⁶ M. Zito,⁶⁶ X. R. Chen,⁶⁷ H. Liu,⁶⁷ W. Park,⁶⁷ M. V. Purohit,⁶⁷ J. R. Wilson,⁶⁷ M. T. Allen,⁶⁸ D. Aston,⁶⁸ R. Bartoldus,⁶⁸ P. Bechtle,⁶⁸ N. Berger,⁶⁸ R. Claus,⁶⁸ J. P. Coleman,⁶⁸ M. R. Convery,⁶⁸ J. C. Dingfelder,⁶⁸ J. Dorfan,⁶⁸ G. P. Dubois-Felsmann,⁶⁸ W. Dunwoodie,⁶⁸ R. C. Field,⁶⁸ T. Glanzman,⁶⁸ S. J. Gowdy,⁶⁸ M. T. Graham,⁶⁸ P. Grenier,⁶⁸ C. Hast,⁶⁸ T. Hryn'ova,⁶⁸ W. R. Innes,⁶⁸ J. Kaminski,⁶⁸ M. H. Kelsey,⁶⁸ H. Kim,⁶⁸ P. Kim,⁶⁸ M. L. Kocian,⁶⁸ D. W. G. S. Leith,⁶⁸ S. Li,⁶⁸ S. Luitz,⁶⁸ V. Luth,⁶⁸ H. L. Lynch,⁶⁸ D. B. MacFarlane,⁶⁸ H. Marsiske,⁶⁸ R. Messner,⁶⁸ D. R. Muller,⁶⁸ C. P. O'Grady,⁶⁸ I. Ofte,⁶⁸ A. Perazzo,⁶⁸ M. Perl,⁶⁸ T. Pulliam,⁶⁸ B. N. Ratcliff,⁶⁸ A. Roodman,⁶⁸ A. A. Salnikov,⁶⁸ R. H. Schindler,⁶⁸ J. Schwiening,⁶⁸ A. Snyder,⁶⁸ J. Stelzer,⁶⁸ D. Su,⁶⁸ M. K. Sullivan,⁶⁸ K. Suzuki,⁶⁸ S. K. Swain,⁶⁸ J. M. Thompson,⁶⁸ J. Va'vra,⁶⁸ N. van Bakel,⁶⁸ A. P. Wagner,⁶⁸ M. Weaver,⁶⁸ W. J. Wisniewski,⁶⁸ M. Wittgen,⁶⁸ D. H. Wright,⁶⁸ A. K. Yarritu,⁶⁸ K. Yi,⁶⁸ C. C. Young,⁶⁸ P. R. Burchat,⁶⁹ A. J. Edwards,⁶⁹ S. A. Majewski,⁶⁹ B. A. Petersen,⁶⁹ L. Wilden,⁶⁹ S. Ahmed,⁷⁰ M. S. Alam,⁷⁰ R. Bula,⁷⁰ J. A. Ernst,⁷⁰ V. Jain,⁷⁰ B. Pan,⁷⁰ M. A. Saeed,⁷⁰ F. R. Wappler,⁷⁰ S. B. Zain,⁷⁰ M. Krishnamurthy,⁷¹ S. M. Spanier,⁷¹ R. Eckmann,⁷² J. L. Ritchie,⁷² A. M. Ruland,⁷² C. J. Schilling,⁷² R. F. Schwitters,⁷² J. M. Izen,⁷³ X. C. Lou,⁷³ S. Ye,⁷³ F. Bianchi,⁷⁴ F. Gallo,⁷⁴ D. Gamba,⁷⁴ M. Pelliccioni,⁷⁴ M. Bomben,⁷⁵ L. Bosisio,⁷⁵ C. Cartaro,⁷⁵ F. Cossutti,⁷⁵ G. Della Ricca,⁷⁵ L. Lanceri,⁷⁵ L. Vitale,⁷⁵ V. Azzolini,⁷⁶ N. Lopez-March,⁷⁶ F. Martinez-Vidal,⁷⁶ D. A. Milanes,⁷⁶ A. Oyanguren,⁷⁶ J. Albert,⁷⁷ Sw. Banerjee,⁷⁷ B. Bhuyan,⁷⁷ K. Hamano,⁷⁷ R. Kowalewski,⁷⁷ I. M. Nugent,⁷⁷ J. M. Roney,⁷⁷ R. J. Sobie,⁷⁷ P. F. Harrison,⁷⁸ J. Ilic,⁷⁸ T. E. Latham,⁷⁸ G. B. Mohanty,⁷⁸ H. R. Band,⁷⁹ X. Chen,⁷⁹ S. Dasu,⁷⁹ K. T. Flood,⁷⁹ J. J. Hollar,⁷⁹ P. E. Kutter,⁷⁹ Y. Pan,⁷⁹ M. Pierini,⁷⁹ R. Prepost,⁷⁹ S. L. Wu,⁷⁹ and H. Neal⁸⁰

(The BABAR Collaboration)

¹Laboratoire de Physique des Particules, IN2P3/CNRS et Université de Savoie, F-74941 Annecy-Le-Vieux, France

²Universitat de Barcelona, Facultat de Física, Departament ECM, E-08028 Barcelona, Spain

³Università di Bari, Dipartimento di Fisica and INFN, I-70126 Bari, Italy

⁴University of Bergen, Institute of Physics, N-5007 Bergen, Norway

⁵Lawrence Berkeley National Laboratory and University of California, Berkeley, California 94720, USA

⁶University of Birmingham, Birmingham, B15 2TT, United Kingdom

⁷Ruhr Universität Bochum, Institut für Experimentalphysik 1, D-44780 Bochum, Germany

⁸University of Bristol, Bristol BS8 1TL, United Kingdom

⁹University of British Columbia, Vancouver, British Columbia, Canada V6T 1Z1

¹⁰Brunel University, Uxbridge, Middlesex UB8 3PH, United Kingdom

¹¹Budker Institute of Nuclear Physics, Novosibirsk 630090, Russia

¹²University of California at Irvine, Irvine, California 92697, USA

¹³University of California at Los Angeles, Los Angeles, California 90024, USA

¹⁴University of California at Riverside, Riverside, California 92521, USA

¹⁵University of California at San Diego, La Jolla, California 92093, USA

¹⁶University of California at Santa Barbara, Santa Barbara, California 93106, USA

¹⁷University of California at Santa Cruz, Institute for Particle Physics, Santa Cruz, California 95064, USA

¹⁸California Institute of Technology, Pasadena, California 91125, USA

¹⁹University of Cincinnati, Cincinnati, Ohio 45221, USA

²⁰University of Colorado, Boulder, Colorado 80309, USA

²¹Colorado State University, Fort Collins, Colorado 80523, USA

²²Universität Dortmund, Institut für Physik, D-44221 Dortmund, Germany

²³Technische Universität Dresden, Institut für Kern- und Teilchenphysik, D-01062 Dresden, Germany

²⁴Laboratoire Leprince-Ringuet, CNRS/IN2P3, Ecole Polytechnique, F-91128 Palaiseau, France

- ²⁵ *University of Edinburgh, Edinburgh EH9 3JZ, United Kingdom*
- ²⁶ *Università di Ferrara, Dipartimento di Fisica and INFN, I-44100 Ferrara, Italy*
- ²⁷ *Laboratori Nazionali di Frascati dell'INFN, I-00044 Frascati, Italy*
- ²⁸ *Università di Genova, Dipartimento di Fisica and INFN, I-16146 Genova, Italy*
- ²⁹ *Harvard University, Cambridge, Massachusetts 02138, USA*
- ³⁰ *Universität Heidelberg, Physikalisches Institut, Philosophenweg 12, D-69120 Heidelberg, Germany*
- ³¹ *Imperial College London, London, SW7 2AZ, United Kingdom*
- ³² *University of Iowa, Iowa City, Iowa 52242, USA*
- ³³ *Iowa State University, Ames, Iowa 50011-3160, USA*
- ³⁴ *Johns Hopkins University, Baltimore, Maryland 21218, USA*
- ³⁵ *Universität Karlsruhe, Institut für Experimentelle Kernphysik, D-76021 Karlsruhe, Germany*
- ³⁶ *Laboratoire de l'Accélérateur Linéaire, IN2P3/CNRS et Université Paris-Sud 11, Centre Scientifique d'Orsay, B. P. 34, F-91898 ORSAY Cedex, France*
- ³⁷ *Lawrence Livermore National Laboratory, Livermore, California 94550, USA*
- ³⁸ *University of Liverpool, Liverpool L69 7ZE, United Kingdom*
- ³⁹ *Queen Mary, University of London, E1 4NS, United Kingdom*
- ⁴⁰ *University of London, Royal Holloway and Bedford New College, Egham, Surrey TW20 0EX, United Kingdom*
- ⁴¹ *University of Louisville, Louisville, Kentucky 40292, USA*
- ⁴² *University of Manchester, Manchester M13 9PL, United Kingdom*
- ⁴³ *University of Maryland, College Park, Maryland 20742, USA*
- ⁴⁴ *University of Massachusetts, Amherst, Massachusetts 01003, USA*
- ⁴⁵ *Massachusetts Institute of Technology, Laboratory for Nuclear Science, Cambridge, Massachusetts 02139, USA*
- ⁴⁶ *McGill University, Montréal, Québec, Canada H3A 2T8*
- ⁴⁷ *Università di Milano, Dipartimento di Fisica and INFN, I-20133 Milano, Italy*
- ⁴⁸ *University of Mississippi, University, Mississippi 38677, USA*
- ⁴⁹ *Université de Montréal, Physique des Particules, Montréal, Québec, Canada H3C 3J7*
- ⁵⁰ *Mount Holyoke College, South Hadley, Massachusetts 01075, USA*
- ⁵¹ *Università di Napoli Federico II, Dipartimento di Scienze Fisiche and INFN, I-80126, Napoli, Italy*
- ⁵² *NIKHEF, National Institute for Nuclear Physics and High Energy Physics, NL-1009 DB Amsterdam, The Netherlands*
- ⁵³ *University of Notre Dame, Notre Dame, Indiana 46556, USA*
- ⁵⁴ *Ohio State University, Columbus, Ohio 43210, USA*
- ⁵⁵ *University of Oregon, Eugene, Oregon 97403, USA*
- ⁵⁶ *Università di Padova, Dipartimento di Fisica and INFN, I-35131 Padova, Italy*
- ⁵⁷ *Laboratoire de Physique Nucléaire et de Hautes Energies, IN2P3/CNRS, Université Pierre et Marie Curie-Paris6, Université Denis Diderot-Paris7, F-75252 Paris, France*
- ⁵⁸ *University of Pennsylvania, Philadelphia, Pennsylvania 19104, USA*
- ⁵⁹ *Università di Perugia, Dipartimento di Fisica and INFN, I-06100 Perugia, Italy*
- ⁶⁰ *Università di Pisa, Dipartimento di Fisica, Scuola Normale Superiore and INFN, I-56127 Pisa, Italy*
- ⁶¹ *Prairie View A&M University, Prairie View, Texas 77446, USA*
- ⁶² *Princeton University, Princeton, New Jersey 08544, USA*
- ⁶³ *Università di Roma La Sapienza, Dipartimento di Fisica and INFN, I-00185 Roma, Italy*
- ⁶⁴ *Universität Rostock, D-18051 Rostock, Germany*
- ⁶⁵ *Rutherford Appleton Laboratory, Chilton, Didcot, Oxon, OX11 0QX, United Kingdom*
- ⁶⁶ *DSM/Dapnia, CEA/Saclay, F-91191 Gif-sur-Yvette, France*
- ⁶⁷ *University of South Carolina, Columbia, South Carolina 29208, USA*
- ⁶⁸ *Stanford Linear Accelerator Center, Stanford, California 94309, USA*
- ⁶⁹ *Stanford University, Stanford, California 94305-4060, USA*
- ⁷⁰ *State University of New York, Albany, New York 12222, USA*
- ⁷¹ *University of Tennessee, Knoxville, Tennessee 37996, USA*
- ⁷² *University of Texas at Austin, Austin, Texas 78712, USA*
- ⁷³ *University of Texas at Dallas, Richardson, Texas 75083, USA*
- ⁷⁴ *Università di Torino, Dipartimento di Fisica Sperimentale and INFN, I-10125 Torino, Italy*
- ⁷⁵ *Università di Trieste, Dipartimento di Fisica and INFN, I-34127 Trieste, Italy*
- ⁷⁶ *IFIC, Universitat de Valencia-CSIC, E-46071 Valencia, Spain*
- ⁷⁷ *University of Victoria, Victoria, British Columbia, Canada V8W 3P6*
- ⁷⁸ *Department of Physics, University of Warwick, Coventry CV4 7AL, United Kingdom*
- ⁷⁹ *University of Wisconsin, Madison, Wisconsin 53706, USA*
- ⁸⁰ *Yale University, New Haven, Connecticut 06511, USA*

(Dated: October 29, 2018)

We present a search for B decays to a charged scalar meson a_0^+ and a π^0 where the a_0^+ decays to an η meson and a π^+ . The analysis was performed on a data sample consisting of 383×10^6 $B\bar{B}$ pairs collected with the BABAR detector at the PEP-II asymmetric-energy B Factory at SLAC. We

find no significant signal and set an upper limit on the product branching fraction $\mathcal{B}(B^+ \rightarrow a_0^+ \pi^0) \times \mathcal{B}(a_0^+ \rightarrow \eta \pi^+)$ of 1.4×10^{-6} at the 90% confidence level.

PACS numbers: 13.25.Hw, 12.39.Mk

The structure of scalar mesons is a subject of some debate [1, 2]. Proposed models include two-quark or four-quark states with potential contributions from glueballs or a molecular admixture of $K\bar{K}$ meson pairs. Measurement of the branching fraction for the mode $B^+ \rightarrow a_0^+ \pi^0$ [3] is expected to provide an effective test of the two- and four-quark models [5]. The Feynman diagrams for the decay in the two-quark case are shown in Figure 1. Those for the four-quark case are similar except for an $s\bar{s}$ pair produced from the vacuum internal to the a_0^+ meson. The color-allowed electroweak tree diagram shown in Figure 1(a) is suppressed for all a_0^+ models since the W^+ is constrained to decay to states of even G -parity (a generalization of C symmetry to cover particle multiplets) within the Standard Model, whereas the a_0^+ has odd G -parity [4]. This diagram is also suppressed due to vector current conservation considerations. Therefore, the color-suppressed tree diagram in Figure 1(b) and the helicity-suppressed electroweak annihilation diagram in Figure 1(c) become important. The gluonic penguin process in Figure 1(d) is highly suppressed and is therefore not expected to contribute significantly.

The amplitudes for the above diagrams depend on the a_0^+ model used; in particular the annihilation diagram is heavily suppressed in a four-quark model. Hence measurement of the branching fraction provides the potential for model discrimination. In the two-quark case, the predicted branching fractions go as high as 2×10^{-7} [5, 6]. However, in the four-quark case the prediction for the branching fraction is an order of magnitude lower.

The branching fraction for the result quoted below will be given in terms of the product $\mathcal{B}(B^+ \rightarrow a_0^+ \pi^0) \times \mathcal{B}(a_0^+ \rightarrow \eta \pi^+)$ since the branching fraction $\mathcal{B}(a_0^+ \rightarrow \eta \pi^+)$ is not well measured, although it is thought to be approximately 85% [1].

The analysis presented in this paper is based on 347 fb^{-1} of data collected at the $\Upsilon(4S)$ resonance with the *BABAR* detector at the PEP-II asymmetric-energy e^+e^- collider located at the Stanford Linear Accelerator Center. This corresponds to $(383 \pm 4) \times 10^6 B\bar{B}$ pairs.

The *BABAR* detector has been described in detail previously [7]. Track parameters of charged particles are measured by a combination of a 5-layer double-sided silicon vertex tracker and a 40-layer drift chamber (DCH), both operating in the 1.5 T magnetic field of a superconducting solenoid. Photons and electrons are identified using a CsI(Tl) electromagnetic calorimeter. Further charged particle identification (PID) is provided by measurements of the average energy loss (dE/dx) in the tracking devices and by an internally-reflecting, ring-imaging Čerenkov detector (DIRC) covering the central region.

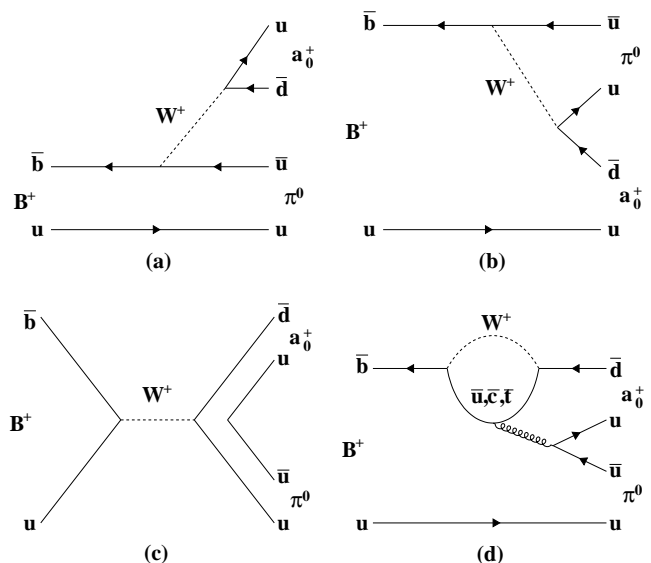


FIG. 1: The Feynman diagrams contributing to the process $B^+ \rightarrow a_0^+ \pi^0$ in the two-quark model. (a) is the external (color-allowed) tree, (b) the internal (color-suppressed) tree, (c) the annihilation process and (d) the gluonic penguin process.

The analysis focuses on a_0^+ mesons produced from the decay $B^+ \rightarrow a_0^+ \pi^0$, followed by $a_0^+ \rightarrow \eta \pi^+$, where the η meson subsequently decays to $\gamma\gamma$ or $\pi^+ \pi^- \pi^0$ final states. The π^0 mesons used are reconstructed via the decay $\pi^0 \rightarrow \gamma\gamma$. The selections used for the analysis are the result of an optimization procedure based on ensemble Monte Carlo (MC) studies. In these studies, a sample of MC candidates is produced for given selection criteria by generating randomly from probability density function (PDF) distributions defined with the selection applied. By re-fitting to the datasets for each set of selection criteria it is possible to select the set that yields the maximum sensitivity to signal. This is done independently for each decay mode considered. In both cases a_0^+ candidates are required to satisfy $0.8 < m_{\eta\pi} < 1.2 \text{ GeV}/c^2$ with the η candidates satisfying $0.51 < m_{\gamma\gamma} < 0.57 \text{ GeV}/c^2$ or $0.540 < m_{3\pi} < 0.555 \text{ GeV}/c^2$. The π^0 produced from the $\eta \rightarrow \pi^+ \pi^- \pi^0$ decay is required to satisfy $0.10 < m_{\pi^0} < 0.16 \text{ GeV}/c^2$. The π^0 daughter of the B candidate is required to satisfy $0.115 < m_{\pi^0} < 0.150 \text{ GeV}/c^2$. This selection is tighter than for the π^0 produced from the η meson since it is of significantly higher energy and therefore has a better resolution. The charged track from the a_0^+ candidate decay is required not to satisfy DIRC- and

DCH-based PID criteria consistent with a kaon hypothesis. This PID selection has been measured to be more than 80% efficient for tracks with momenta up to 4 GeV/ c with a pion mis-identification rate lower than 10% over the same range.

A B meson candidate is characterized kinematically by the energy difference $\Delta E \equiv E_B - \frac{1}{2}\sqrt{s}$ and energy-substituted mass $m_{\text{ES}} \equiv (\frac{1}{4}s - \mathbf{p}_B^2)^{\frac{1}{2}}$, where s is the square of the centre-of-mass energy of the colliding beams, (E_B, \mathbf{p}_B) is the candidate B meson 4-momentum and all values are expressed in the $\Upsilon(4S)$ frame. Signal events peak around zero for ΔE , and at the B meson mass for m_{ES} . The resolutions for ΔE and m_{ES} are approximately 30 MeV and 3 MeV/ c^2 , respectively. We require $|\Delta E| \leq 0.35$ GeV and $5.20 \leq m_{\text{ES}} \leq 5.29$ GeV/ c^2 as an input for the fit used to extract signal and background parameters (described below) in order to maximize the available statistics.

The principal source of background in the analysis arises from random combinations in continuum $e^+e^- \rightarrow q\bar{q}$ ($q = u, d, s, c$) events. These contributions are reduced in part by placing a selection on the variable $|\cos(\theta_{TB})|$, where θ_{TB} is the angle between the thrust axis of the B candidate and the thrust axis of the rest of the event calculated in the $\Upsilon(4S)$ frame. Candidates formed in jet-like $q\bar{q}$ events will peak at $|\cos(\theta_{TB})|$ values approaching 1, whereas signal B decays will follow an almost flat distribution as they are isotropic in this angle. We require $|\cos(\theta_{TB})| < 0.7$ for both η channels. The final variable used in the analysis is a linear Fisher discriminant \mathcal{F} that consists of the angles of the B momentum and B thrust axis (in the $\Upsilon(4S)$ frame) with respect to the beam axis, and the zeroth and second Legendre moments of the energy flow computed with respect to the B thrust axis [8]. The reconstruction efficiencies after selection are presented in Table I.

The analysis uses an extended unbinned maximum-likelihood fit to extract yields for the modes under study. The input variables to the fit are ΔE , m_{ES} , \mathcal{F} and the a_0^+ candidate resonance mass $m_{\eta\pi}$. The extended likelihood function for the fit is defined as:

$$\mathcal{L} = \frac{e^{-(\sum n_j)}}{N!} \prod_{i=1}^N \left[\sum_{j=1}^M n_j \mathcal{P}_j \right], \quad (1)$$

where \mathcal{P}_j is the normalized PDF for a given fit component j . For each candidate i the PDF is evaluated using the fit variables of that candidate. The M fit components are the signal and all background contributions. The total number of candidates is given by N with the yield associated with each fit component given by n_j . The fit for each η channel consists of 16 components modeling signal and continuum candidates separately as well as charged and neutral charmed B meson decays. There are then 12 components modeling individual charmless modes which were found to contribute a background to

the signal. The yields for all B background components are held fixed in the final fit using values calculated from the latest branching fraction estimates [9], whereas the signal and continuum background yields are allowed to vary.

The fit model is constructed in order to extract signal candidates effectively from a sample where multiple reconstruction hypotheses exist for each event. The signal MC events have an average candidate multiplicity of 1.4 for both η decay modes.

In this analysis separate PDFs were used to discriminate between correctly and incorrectly reconstructed signal candidates in MC. This was achieved by using MC information to separate the signal MC candidates into an almost pure sample of correctly reconstructed candidates and a sample consisting mainly of incorrectly reconstructed candidates. By iteratively fitting the separate PDFs to each sample in turn, a consistent set of PDFs for the two cases was obtained. The component for correctly reconstructed candidates was then taken to model signal candidates in the final fit to data. The fraction of events in the MC that were identified as correctly reconstructed by the fit was approximately 62% for both η channels. The signal candidate yield resulting from the fit to MC was verified to be consistent with that expected.

The shapes of the distributions for incorrectly reconstructed signal were found to be similar to continuum background and thus any such candidates are assumed to be absorbed into the yield associated with the continuum PDF. Modeling signal candidates in this way was shown using ensemble MC studies to provide better sensitivity to signal than other methods. As a final test, the method was validated using ensemble MC studies to show that it introduced no bias into the final fit result.

Any continuum and $B\bar{B}$ backgrounds that remain after the event selection criteria have been applied are identified and modeled using Monte Carlo simulation based on the full physics and detector models [10]. Charmless B decays providing a background to the signal are identified by analyzing the MC candidates passing selection from a large mixed sample of Standard Model B decays. Charged and neutral charmed B decays are modeled separately and individual components are included for each charmless B decay mode found to contribute. The PDF parameters for each B background component are obtained from MC samples and held fixed in the final fit to data. Those for the continuum background shape are left free in the final fit. The contributions from two charmless backgrounds with the same final state as signal, those for $B^+ \rightarrow a_0(1450)^+\pi^0$ and non-resonant $B^+ \rightarrow \eta\pi^+\pi^0$, are estimated using fits to the relevant regions of the Dalitz plane. Any potential interference effects were neglected since the fits gave no significant yields for these modes.

The total PDFs are modeled as products of the PDFs for each of the four fit variables. The signal shapes in ΔE , m_{ES} , $m_{\eta\pi}$ and \mathcal{F} are modeled with a Novosi-

TABLE I: The results of the fit to the full data set, and other values required for calculating the branching fraction. All B background yields were held fixed. The upper limit is shown first with only the statistical error and then with the total error.

| Required Quantity/Result | $\eta \rightarrow \gamma\gamma$ | $\eta \rightarrow \pi^+\pi^-\pi^0$ |
|---|---|--|
| Candidates to fit | 103054 | 31626 |
| Fixed B Background (candidates) | 1640 | 942 |
| Signal Yield (candidates) | -8 ± 19 | 13 ± 13 |
| Continuum Yield (candidates) | 101400 ± 300 | 30700 ± 200 |
| ML Fit Bias (candidates) | 5.2 ± 3.0 | -2.0 ± 1.3 |
| Efficiencies and BFs | | |
| Efficiency (%) | 16.3 ± 0.1 | 10.2 ± 0.1 |
| $\mathcal{B}(\eta \rightarrow X)$ (%) | 39.4 ± 0.3 | 22.6 ± 0.4 |
| Branching Fraction ($\times 10^{-6}$) | $-0.6^{+0.8}_{-0.7}$ (stat) $^{+0.4}_{-0.3}$ (syst) | $1.7^{+1.6}_{-1.4}$ (stat) $^{+0.3}_{-0.4}$ (syst) |
| Combined Mode Results | | |
| Branching Fraction ($\times 10^{-6}$) | $0.1^{+0.7}_{-0.7}$ (stat) $^{+0.3}_{-0.3}$ (syst) | |
| Significance | 0.1σ (stat + syst) | |
| Upper Limit 90% C.L. ($\times 10^{-6}$) | < 1.3 (statistical error only) | |
| Upper Limit 90% C.L. ($\times 10^{-6}$) | < 1.4 (total error) | |

birsk [11] function, the sum of two independent Gaussians, a Breit-Wigner, and an asymmetric Gaussian, respectively. The signal parameters used for the a_0^+ lineshape are a Breit-Wigner peak value of $983 \text{ MeV}/c^2$ with a width of $79 \text{ MeV}/c^2$. These were used in the MC simulation and are consistent with previous analyses [12], although the width is considered to be uncertain over a conservative range of $50\text{-}100 \text{ MeV}/c^2$ in the evaluation of systematic error. Slowly-varying background distributions in \mathcal{F} and $m_{\eta\pi}$ are modeled with Chebychev polynomials of the appropriate order. Such polynomials are also used for ΔE in the charmed B and continuum background cases. For these components m_{ES} is modeled with an ARGUS [13] threshold function. In the case of charmless B backgrounds, ΔE and m_{ES} are modeled 2-dimensionally using non-parametric PDFs [14], so as to model correlations between the two variables. Studies of the MC samples for each mode have shown that these correlations can be as high as 29%.

The results of the analysis are presented in Table I. The statistical errors on the signal yields are defined using the change in the central value when the quantity $-2 \ln \mathcal{L}$ increases by one unit from the minimum. The significance is taken as the square root of the difference between the value of $-2 \ln \mathcal{L}$ for zero signal and the value at the minimum (including additive systematics).

For the purposes of the branching fraction calculation we assume that the $\Upsilon(4S)$ decays with an equal rate to both B^+B^- and $B^0\bar{B}^0$ [15]. The fit bias is measured using an ensemble MC study based on a parameterization taken from the fit to data with all yield values taken from data. Where a negative yield is found a value of zero is used for the study. The branching fraction results from the two η decay modes are combined by forming the product of the likelihood functions, after their maxima have

been shifted to account for fit bias. The functions themselves are defined by computing the likelihood values for signal yields around the maximum. Systematic errors are included at the required stages in the calculation depending on correlations between the two η channels.

We find no significant signal in either η decay mode and thus quote upper limits on the branching fraction at the 90% confidence level (C.L.), taken to be the branching fraction below which lies 90% of the total of the likelihood integral in the positive branching fraction region.

In Figure 2 we show projections of each of the four fit variables for both the $\eta \rightarrow \gamma\gamma$ and $\eta \rightarrow \pi^+\pi^-\pi^0$ decay modes. To enhance the visibility of a potential signal, the candidates in these figures have been required to satisfy the condition that the likelihood ratio $\mathcal{L}_{sig}/[\mathcal{L}_{sig} + \Sigma \mathcal{L}_{bkg}]$ for any candidate be greater than 0.6. Here \mathcal{L}_X is the likelihood for a given event being described by either the signal or background model. The likelihoods are calculated for each figure separately, excluding the variable being plotted. As can be seen there is no significant signal peak for either mode.

The largest sources of systematic uncertainty in the analysis arise from poor knowledge of the a_0^+ lineshape and from the error in the estimated background contributions. By varying the width of the a_0^+ Breit-Wigner between 50 and $100 \text{ MeV}/c^2$ we predict an uncertainty of approximately +5 and -4 candidates for $\eta \rightarrow \gamma\gamma$ and +0.5 and -1 candidate for $\eta \rightarrow \pi^+\pi^-\pi^0$. Varying the charmless yields within their branching fraction errors (or $\pm 100\%$ where a limit is used), and the charmed B yields by $\pm 10\%$, gives an estimated uncertainty of ± 4 candidates in $\eta \rightarrow \gamma\gamma$ and ± 1 candidate in $\eta \rightarrow \pi^+\pi^-\pi^0$. The error due to the uncertainty in the fit bias was calculated as the sum in quadrature of 50% of the measured bias and its statistical error, as taken from the ensemble MC

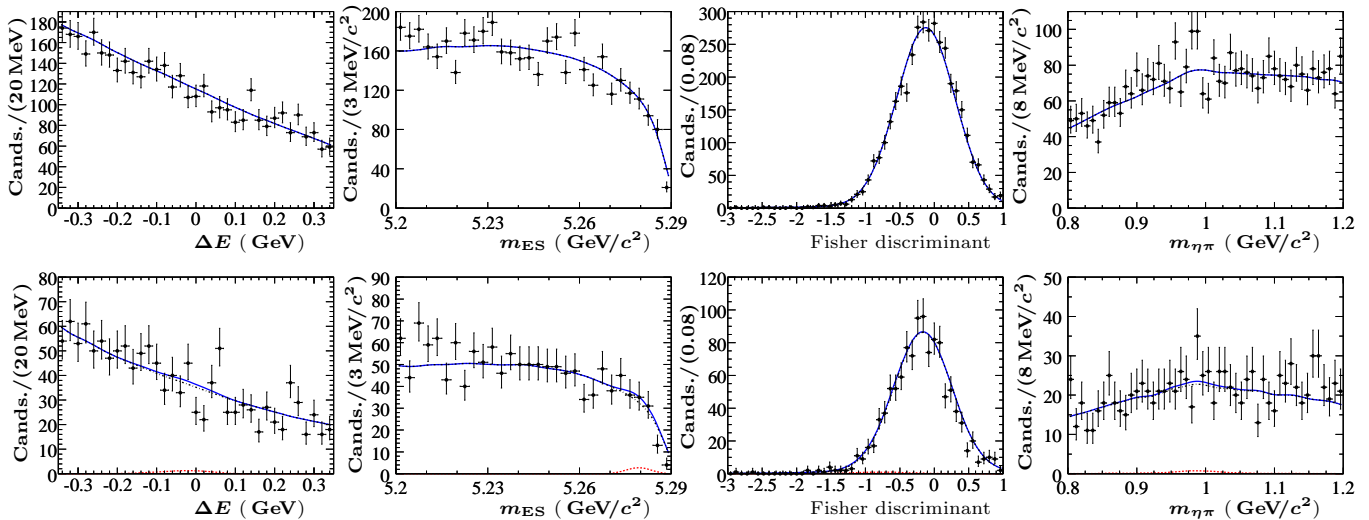


FIG. 2: Likelihood-ratio-enhanced projections for the four fit variables (left to right) for the $\eta \rightarrow \gamma\gamma$ (top) and $\eta \rightarrow \pi^+\pi^-\pi^0$ (bottom) cases. Experimental data are represented by points with error bars, solid blue curves represent the full fit model. For the $\eta_{3\pi}$ case, the combined background component is represented by the black dash-dotted curve and the signal component by the red dashed curve. The efficiency of the likelihood ratio selection on the signal component in the $\eta_{3\pi}$ case is 80.8%.

TABLE II: Estimated systematic errors in the final fit result. Error sources which are Correlated and Uncorrelated for the two η decay modes are denoted by [C] and [U], respectively.

| Source of Uncertainty | $\eta \rightarrow \gamma\gamma$ | $\eta \rightarrow \pi^+\pi^-\pi^0$ |
|--|---------------------------------|------------------------------------|
| Additive (Candidates) | | |
| Fit Parameters [U] | +5.9 -4.4 | +0.5 -1.8 |
| Charmless Yields [U] | +3.6 | +1.2 |
| Charm Yields [U] | -3.7 +0.2 | -1.2 +0.2 |
| Fit Bias [U] | -0.3 ± 3.0 | -0.2 ± 1.3 |
| Total Additive (Candidates) | +7.5 -6.5 | +1.9 -2.6 |
| Multiplicative (%) | | |
| Neutral Efficiency [C] | ± 6.0 | ± 6.0 |
| Tracking Efficiency [C] | ± 0.5 | ± 1.4 |
| $ \cos(\theta_{TB}) $ Selection [C] | ± 3.0 | ± 3.0 |
| MC Statistics [U] | ± 0.4 | ± 0.3 |
| Number of $B\bar{B}$ Events [C] | ± 1.1 | ± 1.1 |
| Daughter η Decay BF [U] | ± 0.7 | ± 1.8 |
| Total Multiplicative (%) | ± 6.9 | ± 7.2 |
| Total BF Syst Error ($\times 10^{-6}$) | +0.4 -0.3 | +0.3 -0.4 |

study described above. This value was calculated to be approximately ± 3 candidates in the $\eta \rightarrow \gamma\gamma$ channel and ± 1 candidate for $\eta \rightarrow \pi^+\pi^-\pi^0$.

Further sources of systematic uncertainty, which are multiplicative rather than additive, affect the efficiency and thus enter into the branching fraction calculation. Limited signal MC statistics account for 0.4% in both η decay modes. Auxiliary studies on inclusive control samples [8], predict errors of 0.5% per charged track and 3% per reconstructed η or π^0 decaying to two photons. The estimate of the number of produced $B\bar{B}$ events is uncer-

tain by 1.1%. The uncertainties in B daughter product branching fractions are taken to be 2% for $\eta \rightarrow \gamma\gamma$ and 3% for $\eta \rightarrow \pi^+\pi^-\pi^0$ [9]. A summary of all systematic error contributions is presented in Table II.

In conclusion, we do not find a significant signal for the mode $B^+ \rightarrow a_0^+\pi^0$. We set an upper limit at 90% C.L. on the branching fraction $\mathcal{B}(B^+ \rightarrow a_0^+\pi^0) \times \mathcal{B}(a_0^+ \rightarrow \eta\pi^+)$ of 1.4×10^{-6} , suggesting that there is insufficient sensitivity with the current dataset to probe the predicted theoretical parameter space, with the largest predicted branching fraction being 2×10^{-7} [5]. We are therefore unable to comment on the validity of any of the current models of the a_0^+ .

We are grateful for the excellent luminosity and machine conditions provided by our PEP-II colleagues, and for the substantial dedicated effort from the computing organizations that support BABAR. The collaborating institutions wish to thank SLAC for its support and kind hospitality. This work is supported by DOE and NSF (USA), NSERC (Canada), IHEP (China), CEA and CNRS-IN2P3 (France), BMBF and DFG (Germany), INFN (Italy), FOM (The Netherlands), NFR (Norway), MIST (Russia), MEC (Spain), and STFC (United Kingdom). Individuals have received support from the Marie Curie EIF (European Union) and the A. P. Sloan Foundation.

* Deceased

† Now at Tel Aviv University, Tel Aviv, 69978, Israel

‡ Also with Università di Perugia, Dipartimento di Fisica,

Perugia, Italy

[§] Also with Università della Basilicata, Potenza, Italy

[¶] Also with Universitat de Barcelona, Facultat de Física, Departament ECM, E-08028 Barcelona, Spain

- [1] Particle Data Group, Y.-M. Yao *et al.*, *J. Phys.* **G33**, 1 (2006), “Note on Scalar Mesons”, p. 546.
- [2] V. Baru *et al.*, *Phys. Lett. B* **586**, 53 (2004).
- [3] Throughout this paper, charged-conjugate decays are also implied.
- [4] S. Laplace and V. Shelkov, *Eur. Phys. Jour. C* **22**, 431 (2001).
- [5] D. Delepine, *et al.*, *Eur. Phys. Jour. C* **45**, 693 (2006).
- [6] H.-Y. Cheng, *et al.*, *Phys. Rev. D* **73**, 014017 (2006).
- [7] BABAR Collaboration, B. Aubert *et al.*, *Nucl. Instrum. Methods Phys. Res., Sect. A* **479**, 1 (2002).
- [8] BABAR Collaboration, B. Aubert *et al.*, *Phys. Rev. D* **70**, 032006 (2004).
- [9] Particle Data Group, Y.-M. Yao *et al.*, *J. Phys.* **G33**, 1 (2006); Heavy Flavour Averaging Group (HFAG), E. Barberio, *et al.*, hep-ex/0603003 (2006).
- [10] The BABAR detector Monte Carlo simulation is based on GEANT4: S. Agostinelli *et al.*, *Nucl. Instrum. Methods Phys. Res., Sect. A* **506**, 250 (2003).
- [11] The Novosibirsk function is defined as $f(x) = A_s \exp(-0.5(\ln^2[1 + \Lambda\tau(x - x_0)]/\tau^2 + \tau))$ where $\Lambda = \sinh(\tau\sqrt{\ln 4})/(\sigma\tau\sqrt{\ln 4})$, the peak is x_0 , τ is the tail parameter and A_s is a normalization factor.
- [12] E852 Collaboration, S. Teige *et al.*, *Phys. Rev. D* **59**, 012001 (1998).
- [13] ARGUS Collaboration, H. Albrecht, *et al.*, *Phys. Lett. B* **241**, 278 (1990); Function defined as $f(x) = Nx[(1 - (x/E_{beam}))^2 \exp[p(1 - (x/E_{beam}))^2]]^{1/2}$, where N is a normalization factor, p a shape parameter and E_{beam} is 50% of the centre-of-mass energy of the colliding beams.
- [14] K. S. Cranmer, *Comput. Phys. Commun.* **136**, 198 (2001).
- [15] See for instance BABAR Collaboration, B. Aubert *et al.*, *Phys. Rev. D* **69**, 071101 (2004), and references therein.